Accepted version

Di Mariano A., AMOROSO S., Arroyo M., Monaco P., Gens A. (2019). “Case Study: SDMT-based numerical analyses of a deep excavation in soft soil”, ASCE Journal of Geotechnical and Geoenvironmental Engineering, ISSN 1090-0241. 145(1), 04018102, 12 pp. doi: 10.1061/(ASCE)GT.1943-5606.0001993. American Society of Civil Engineers, Reston, VA, USA. [Web of Science: WOS:000450402300003, Scopus: 2-s2.0-85056464989]

Case Study: SDMT-based numerical analyses of a deep excavation in soft soil

Alessandra Di Mariano
Staff Scientist, International Center for Numerical Methods in Engineering (CIMNE), Barcelona, Spain
ORCID: 0000-0001-7334-4486

Sara Amoroso
Researcher, Istituto Nazionale di Geofisica e Vulcanologia, L'Aquila, Italy
ORCID: 0000-0001-5835-079X
Corresponding author, e-mail: sara.amoroso@ingv.it

Marcos Arroyo
Professor, Dept. of Civil and Environmental Engineering, Geosciences Division, Universitat Politècnica de Catalunya (UPC), Barcelona, Spain
ORCID: 0000-0001-9384-9107

Paola Monaco
Associate Professor, Dept. of Civil, Architectural and Environmental Engineering, University of L'Aquila, L'Aquila, Italy
ORCID: 0000-0002-1473-158X

Antonio Gens
Professor, Dept. of Civil and Environmental Engineering, Geosciences Division, Universitat Politècnica de Catalunya (UPC), Barcelona, Spain
ORCID: 0000-0001-7588-7054

Abstract

The paper explores the application of conventional (DMT) and seismic (SDMT) dilatometer tests to the important case of deep excavation design. The work presents finite element (FE) analyses simulating a deep excavation close to Barcelona (Spain). A thick layer of soft interbedded sandy and silty soils made characterization based on laboratory testing very difficult. SDMT offered an alternative to estimate the soil stiffness and its stress-strain dependency. Numerical results and high quality monitoring data show quite close agreement for most phases of the construction process, thus supporting the use of seismic dilatometer tests in the numerical analyses of deep excavations. The paper also indicates the importance of incorporating stiffness data at low strains. FE analyses involved some uncertainties derived from the presence of jet-grouting soil treatments. On this point, a parametric study illustrates the effects of different modeling approaches.

Author keywords: nonlinear soil stiffness, seismic dilatometer, finite element analysis, deep excavation, monitoring, jet-grout

1. Introduction

Deep excavations in urban areas generally induce ground movements that may damage adjacent structures. Those movements are quite sensitive to a number of factors, such as soil mechanical properties, excavation geometry, retaining wall characteristics, construction sequences and construction methods. Accurate evaluation of soil movements is an important aspect to manage third-party risks (Arroyo et al. 2007). Numerical analyses are nowadays the tool of choice for estimating deep excavation induced displacements (Yoo et al. 2014, Dias and Bejuizen 2013). They are particularly necessary when design includes special features (e.g. ground improvement) that are poorly represented in empirical databases (Ou 2016).

It is generally acknowledged that soil stiffness nonlinear dependency on strains should be properly taken into account in the analysis of geotechnical structures (Burland 1989). This is especially true for the specific case of deep excavations induced displacements (St John et al. 1993, Hashash and Whittle 1996, Jardine et al. 2005, Brinkgreve et al. 2006, Finno 2010, Ou 2016). Several constitutive models can capture stiffness dependence on stress-strain levels in a realistic manner and many of them are readily available in commercial software. However, calibration of a significant number of parameters is a necessary step for their application. Generally, model calibrations may be based on laboratory testing, but obtaining good stiffness data from it requires high quality samples and careful testing procedures (e.g. Cho and Finno 2009). For gravels, sands and silts, obtaining unaltered samples for testing in laboratories is a very difficult task. Inverse analysis of monitoring measurements appears as a rational alternative when data is scarce (Ledesma et al. 1996, Calvello and Finno 2004, Hashash et al. 2006). However, inverse analysis and soil testing work best together (Finno 2010). Trial sections (Arroyo et al. 2007) are ideal for model calibration but when they are not available, the model has to be adjusted as the excavation proceeds.

When laboratory testing is difficult, one possible alternative is to rely on in-situ tests. Not all in-situ tests are equally suitable for this purpose. The relatively cheap standard penetration test (SPT) is a strength related test with poor repeatability. Khoiri and Ou (2013) state that stiffness parameters obtained from excavation back-analyses may not be correlated to SPT. On the contrary, self-boring pressuremeter tests (SBPM) may be used to fit a whole stiffness degradation curve, particularly when including unload-reload loops (Jardine 1992, Fahey and Carter 1993). Nevertheless, they are quite sensitive to operational details and not frequently available. Two in-situ tests that are repeatable, easily available and allow deriving soil stiffness decay curves are the seismic cone penetration test (SCPT) and the seismic dilatometer test (SDMT). Indeed, they both allow obtaining small-strain modulus measurements determined from seismic shear wave velocities. While it is very difficult to obtain reliable operative stiffness values from CPT (Been et al. 2010), those values

77 deduced from DMT can actually give good settlement predictions (Monaco et al. 2007, Monaco et
78 al. 2014).
79 Several researchers (Mayne et al. 1999, Lehane and Fahey 2004, Marchetti et al. 2008, Amoroso
80 et al. 2013, Amoroso et al. 2014, Cox and Mayne 2015, Pepe at al. 2015, Rodrigues et al. 2016,
81 Bosco and Monaco 2016) have presented procedures to calibrate stiffness degradation curves using
82 seismic dilatometer tests (SDMTs). Despite that, relatively little work has investigated the
83 performance of SDMT-calibrated stiffness values in numerical analyses. Arroyo et al. (2008)
84 presented initial results for a trial section in a cut-and-cover railway tunnel in Barcelona, but both
85 monitoring and SDMT results were incomplete. Later, Sau et al. (2012) reanalyzed the case with
86 improved data, but they did not use a constitutive model representing soil small strain behavior.
87 A new case history is here analyzed, with more complete SDMT and monitoring data, using a
88 constitutive model with appropriate representation of soil stiffness degradation curves. In the paper,
89 numerical results are compared with monitoring data and their significance is discussed by means of
90 a parametric study.
91
92 **2. Case description**
93 Verge de Montserrat Station (recently renamed "Les Moreres") is a tube station of the Line 9
94 (L9) connecting Barcelona city center to its airport. The site is located within the Llobregat River
95 Delta, an area dominated by Holocene soft deposits with the ground water table always close to the
96 soil surface. The construction of the station required an 18.5 m deep excavation. The station plan is
97 approximately cruciform and its dimensions are shown in Fig. 1, whereas Fig. 2 illustrates a
98 geotechnical cross section. Several buildings are present near the station. The closest one, at 9 m
99 from the diaphragm walls (Fig. 1), is a six-storey building whose plan area is 51 m long and 23 m
100 wide, founded on a 0.7 m thick reinforced concrete slab. The building is composed of three blocks
101 separated by two full-height expansion joints that extend from roof to ground-floor levels. Precise

estimates of excavation-induced movements were required to assess any potential damage to the building, as well as to evaluate appropriate safety measures during excavation.

2.1. Geotechnical conditions

The general geological structure of the Llobregat Delta (Gámez 2007) is similar to that of other Mediterranean Deltas. A wedge of low plasticity silty and clayey deposits, (UG5, UG6, UG7 and UG8 in the cross section of Fig. 2), growing up to a thickness of 60 m near the shoreline, overlies a deep sandy and gravelly aquifer (below UG8 in Fig. 2) and, in turn, it is overlaid by a roughly 10 m thick, well graded, medium dense sand (UG2, UG3 and UG4 in Fig. 2). A superficial thin deposit of alluvial fine silts (UG1 in Fig. 2) sometimes appears on top, as well as a variable thickness of made ground. Previous experiences clearly indicate that most geotechnical problems in the area are associated to the compressibility of the intermediate wedge of low plasticity soft soil (Gens et al. 2006). These critical silty and clayey layers pose great sampling difficulties, due to the presence of finely interbedded sandy layers (Pineda et al. 2012). As a result, intact samples recovery from boreholes is very challenging and laboratory measurements of in-situ stiffness parameters are scarce and unreliable. For large projects, some authors (Gens and Lloret 2003, Arroyo et al. 2007) have conducted full-scale instrumented load tests to overcome such inconveniences. Unfortunately, this was not a feasible option for the present case and design had to rely just on site investigations. There were encouraging precedents in the area of DMT use for embankment induced settlement prediction (Arroyo and Mateos 2006), suggesting that good results could also be obtained for other problems.

Fig. 1 illustrates the site investigation layout for the station. Initial investigations included boreholes (S3.9, SM-014, SA, SB, SC) and piezocone tests (CPTu1, CPTu2, respectively 42 and 44 m deep), which registered the phreatic level at 3.5 m depth. A second round of site investigations included flat (DMT1, DMT2, respectively 39 and 40 m deep) and seismic dilatometer tests (SDMT3, SDMT4, respectively 44 and 42 m deep). Descriptive columns from these boreholes,

identification data from disturbed samples recovered from boreholes, as well as CPTu data may be found online as Supplemental Data to this paper (Table S1, Fig. S1). All these data were jointly considered during design and construction; however, for the purposes of this study, we proceeded, as far as possible, as if only the SDMT data were available.

Fig. 3 shows the profiles of DMT indices, namely the material index I_D and the horizontal stress index K_D, and of the constrained modulus M (also designated as M_{DMT}) obtained from DMT1, DMT2, SDMT3 and SDMT4 (Marchetti 1980). The profiles of the shear wave velocity V_S were determined from SDMT3 and SDMT4, while the corrected cone resistance q_t from CPTu1 and CPTu2. Results show similar patterns across the whole area of study, nevertheless the variability in detail is significant due to the fine interlayering of silts, sands and clays, which represents the major feature of the soil profile.

To define a geotechnical model for the 2D section indicated in Figs. 1 and 2, average values of the closest investigations available were used. Fig. S2 of Supplemental Data shows average profiles of I_D, M, K_D, V_S and small strain shear moduli G_0. The soil profile interpreted from the DMT/SDMT data was later used in all numerical analyses. It includes 2 m of made ground (R) overlying a thin layer of fine silts (UG1) (between 2.0 and 4.0 m depth), followed by another thin stratum (UG2) of fine sands with some gravel intercalations (down to about 5.5 m depth) and then again by fine sands (UG3) (down to 9.8 m depth). Below, a combination of layers of sandy silts (UG4), silty clays with some sandy intercalations (UG5), sandy silts (UG6) and clays and silts (UG7) is encountered down to a depth of approximately 40 m. Finally, silty sands (UG8) form the last layer identified from in-situ tests, below which a stratum of gravels hosts a confined aquifer. Other authors (Arroyo et al. 2004, Gens et al. 2011) have reported similar soil profiles in nearby sites.

2.2. Construction activities

The station was built within diaphragm walls made of discrete panels of about 3.5 m length, 1.2 m width and 34 m depth. The walls were executed before the main tube line tunnel, which in turn

was built (with a 9.4 m diameter EPB machine) before starting the excavation. Verge de Montserrat station was constructed by the top-down construction method, being its main roof slab at a depth of 2.4 m from the ground surface and its second slab 5 m below the main roof slab.

Jet-grouted bottom plugs have frequently been used for deep excavations in the Llobregat Delta area (Eramo et al. 2011), not only to avoid any heave or piping risk in the interbedded silty deposits but also to reduce wall displacements. In this case, a 3 m thick jet-grouted slab was executed before the excavation just beneath the tunnel invert, at a depth of approximately 18 m. In addition, jet-grout columns were executed outside the wall box (once it was completed) on the side adjacent to the building, so to reduce accidental piping risk through diaphragm wall panels. Each of these columns, whose center is at 0.30 m distance from the wall panels, has a nominal diameter of 2.0 m and a length of about 23 m, starting from a depth of nearly 4 m from the ground surface.

Before works started, dewatering within the walls was performed to facilitate all operations and as an additional safeguard against any bottom slab leaks. Table 1 summarizes the complete sequence of all construction activities for the Verge de Montserrat Station.

2.3. Monitoring

Buildings, ground surface and subsurface displacements, pore water pressures as well as diaphragm wall movements were monitored at all times during the construction works.

The section represented in the numerical model includes topographic targets, one inclinometer tube in the diaphragm wall, one extensometer and some piezometers (Fig. 2). The execution of the jet-grout columns behind the diaphragm wall panels (phase E) damaged both the extensometer and the inclinometer in this section. They were reinstalled just after the construction of the main roof slab (phase H). For this reason, comparisons of computed and observed movements focus on the subsequent excavation phases.

3. Numerical analyses

All numerical analyses were performed with the Plaxis 2D Finite Element Program (Brinkgreve et al. 2008). First, the characteristics and results of a reference case (Base Case) are presented and then different modeling hypotheses are explored through parametric analyses.

3.1. Model set-up: Base Case

3.1.1. Geometry and boundary conditions

All numerical analyses refer to a representative section of the station that is perpendicular to the tunnel longitudinal axis and near the 6-storey building shown in Fig. 1. In this location, three-dimensional effects should play a relatively small role for two main reasons. First, the length to depth ratio of the excavation (L/H_e) is never below 6 and second, the out-of-plane motion is restricted due to the presence of very stiff transverse walls in the lateral arm of the station, closer to the building long wall (Fig. 1). The model includes all geotechnical units (UG1, UG2, UG3, UG4, UG5, UG6, UG7 and UG8) identified in the Quaternary deposits from the in-situ tests and two extra units, the fill layer (R) and the jet-grouted bottom strut (JG).

The model width is ten times wider than the excavation (170 m wide) and the position of the mesh lower boundary (at 44 m depth) coincides with the stiff layer of gravels, where in-situ tests found refusal. In the two vertical lateral boundaries, the horizontal displacements are set equal to zero and the lower boundary is fixed (i.e. both horizontal and vertical displacements are nil). Fifteen-node triangular elements were used to model soil layers, while five-node Mindlin beam elements were used to represent diaphragm walls, station slabs, the tunnel lining and the slab of the six-storey building. Hinged connections link tunnel slabs with diaphragm walls, a continuous concrete ring represents the tunnel lining, while three independent elastic beam elements reproduce the six-storey building blocks separated by expansion joints. A uniformly distributed surface load of 60 kPa, applied to these beam elements, takes into account the weight of the building. Finally, elastoplastic interface elements take into account soil-structure interactions. Table 2 contains all

structures mechanical characteristics, namely the axial stiffness, *EA*, flexural stiffness *EI*, element thickness *d*, Poisson's ratio υ and weight of the structure per unit length *w*.

3.1.2. Initial conditions

The initial phreatic level is horizontal and located at a depth of 3.5 m from the ground surface. The initial pore pressure distribution is hydrostatic and the diaphragm walls as well as the tunnel lining are impermeable.

From DMT interpretation, all Quaternary deposits appear to be quasi-normally consolidated (overconsolidation ratio *OCR*=1-1.2), except for the uppermost layer (UG1) where seasonal drying is a likely cause for some overconsolidation. The initial state of stress in the ground was thus determined by normally consolidated loading conditions.

3.1.3. Constitutive model calibration

Tables 3 to 5 summarize the mechanical parameters used in the numerical analyses to characterize each geotechnical unit (UG). The values of hydraulic conductivity (*K*) were obtained from pumping tests and applied in previous numerical studies (Garitte et al. 2010). All natural soil layers were modelled as nonlinear elastoplastic materials, using the Hardening Soil Model with Small strain stiffness (HSSmall, Benz 2007). On the other hand, a simple linear elastic-perfectly plastic constitutive model with a Mohr-Coulomb failure criterion is used for both the fill layer (R) and the jet-grouting bottom slab (JG).

The soil parameters that are more significant for the evaluation of excavation-induced displacements in conditions far away from failure are those related to stiffness. In the HSSmall model, the stiffness related parameters include four reference moduli E_{oed}^{ref}, E_{50}^{ref}, E_{ur}^{ref}, G_0^{ref}, which represent respectively the tangent stiffness modulus for primary oedometer loading, the secant modulus in standard drained triaxial tests, the unloading/reloading modulus at operative strains and the reference shear modulus at small strains:

231

$$E_{oed} = E_{oed}^{ref} \left\{ \left(c \cdot \cot\varphi + \sigma_1^{'} \right) / \left(c \cdot \cot\varphi + p_{ref} \right) \right\}^m \quad (1)$$

$$E_{50} = E_{50}^{ref} \left\{ \left(c \cdot \cot\varphi + \sigma_3^{'} \right) / \left(c \cdot \cot\varphi + p_{ref} \right) \right\}^m \quad (2)$$

$$E_{ur} = E_{ur}^{ref} \left\{ \left(c \cdot \cot\varphi + \sigma_3^{'} \right) / \left(c \cdot \cot\varphi + p_{ref} \right) \right\}^m \quad (3)$$

$$G_0 = G_0^{ref} \left\{ \left(c \cdot \cot\varphi + \sigma_3^{'} \right) / \left(c \cdot \cot\varphi + p_{ref} \right) \right\}^m \quad (4)$$

232

233 In Eqs. (1) - (4), m is a parameter controlling stress-level stiffness dependency, σ'_1 and σ'_3 are
234 the major and minor principal effective stresses, while p_{ref} is a reference pressure of 100 kPa and c
235 is the effective cohesion.

236 Marchetti (1980) defined the DMT constrained modulus M_{DMT} as:

237

$$M_{DMT} = R_M \cdot E_D \quad (5)$$

238

239 where R_M is a factor dependent on K_D and I_D, and E_D is the dilatometer modulus.

240 Arroyo et al. (2004) had shown that for the silty and clayey units present in the area, laboratory
241 determinations of constrained modulus compared well with M_{DMT}. Therefore, in this study, it is
242 assumed $E_{oed} = M_{DMT}$, and the DMT constrained modulus M_{DMT} is employed as the basic reference
243 stiffness parameter (Monaco and Marchetti 2004, Arroyo et al. 2008). Also, according to
244 indications given by Vermeer (2001), the following moduli ratios are adopted: $E_{50}^{ref} = E_{oed}^{ref}$,
245 $E_{ur}^{ref} = 4E_{oed}^{ref}$. Finally, the small strain shear modulus G_0 is directly determined from the shear wave
246 velocity V_S, using the theory of elasticity.

247 For every soil layer identified, the M and G_0 profiles obtained from SDMT are employed to infer
248 m (rate of increase of moduli with stress), E_{oed}^{ref} and G_0^{ref} (moduli at reference stresses of 100 kPa).
249 Average values of E_{oed}^{ref} and G_0^{ref} are estimated for each geotechnical unit and average values of E_{oed}

and G_0 are introduced in all numerical analyses. Fig. 4 shows the comparison between E_{oed}, G_0 values obtained from DMT/SDMT and E_{oed}, G_0 values adopted in the FEM analyses. According to Amoroso et al. (2014), SDMT tests provide both small strain and working strain moduli, G_0 and G_{DMT}, at each depth. As suggested by Marchetti et al. (2008), working strain shear moduli G_{DMT} can be derived from constrained moduli M_{DMT} by referring to linear elasticity. As a first approximation:

$$G_{DMT} = \frac{1-2\nu}{2(1-\nu)} M_{DMT} \tag{6}$$

where υ is the Poisson's ratio, assumed equal to 0.2 for all layers. A further step in the calibration of the HSSmall model requires nonlinear stiffness-strain degradation curves for all units. For that purpose, the hyperbolic stress-strain relationship expressed by Eq. (7) can be used (Amoroso et al. 2014):

$$\frac{G}{G_0} = \frac{1}{1+\left(\frac{G_0}{G_{DMT}}-1\right)\frac{\gamma}{\gamma_{DMT}}} \tag{7}$$

In Eq. (7), G is the shear modulus, γ the shear strain, and γ_{DMT} the shear strain associated with working strain DMT moduli. Amoroso et al. (2014) proposed values of γ_{DMT} in the range 0.015-0.30% for sands, in the range 0.23-1.75% for silts and/or clays and greater than 2% for soft clays.

The SDMT profiles provide first order estimates of G_0/G_{DMT} ratios for each geotechnical unit. In this case, DMT shear strains (γ_{DMT}) of 0.1% are assumed in sandy layers (UG2, UG3 and UG4) and of 0.75% in fine-grained geotechnical units (UG1, UG5, UG6, UG7 and UG8). The intersection of the $0.722 \cdot G_0$ horizontal line with the estimated normalized stiffness degradation curve provides the threshold shear strain value referred to in the model as $\gamma_{0.7}$ (Fig. 5).

Apart from the stiffness related parameters, Table 3 reports other parameters that were also estimated using well-established DMT correlations. Thus, the total unit weight (γ) was estimated using the chart developed by Marchetti and Crapps (1981) and the friction angle (φ) for granular layers (UG2, UG3 and UG4) through the following equation (Marchetti 1997):

$$\varphi = 28° + 14.6° \log K_D - 2.1° \log^2 K_D \quad (8)$$

For granular layers the coefficient of earth pressure at rest (K_0^{nc}) was determined through Jaky's expression ($K_0 = 1 - \sin\varphi$). For fine-grained layers, it was estimated from the DMT results using the following expression (Marchetti 1980):

$$K_0^{nc} = (K_D / 1.5)^{0.47} - 0.6 \quad (9)$$

Finally, the effective friction angles for fine-grained layers were selected in agreement with previously reported values for the area (Arroyo et al. 2007, Di Mariano et al. 2007, Gens et al. 2011), as were the parameters for the fill layer (Table 4). Parameter values for the jet-grout are discussed in a separate section.

The FEM code incorporates a coupled hydro-mechanical formulation and, for simplicity, in the Base Case the more sandy upper layers (R, UG1, UG2, UG3 and UG4) are assigned drained behavior while the more clayey/silty lower ones (UG5, UG6, UG7 and UG8) are designated as undrained. A parametric study helps exploring the implications of this choice.

3.1.4. Construction sequence

All FEM analyses reproduce the construction sequence described in Table 1 up to phase N (excavation to deepest level). The EPB tunnel excavation (phase D) is simulated through the contraction method (Brinkgreve et al. 2008), using a soil volume loss of 0.2%, as it was observed

295 on site during the EPB drive (Gens et al. 2011). Excavation processes within the diaphragm walls
296 are modeled by incrementally removing solid soil elements. All construction phases (A-N in Table
297 1) are carried out as elastic-plastic deformation analyses and are defined as plastic calculations.
298 In the dewatering phases, I and M, the pore pressure distribution is evaluated prior to the plastic
299 calculation using the Staged construction mode. New hydraulic boundary conditions are defined in
300 which the pumping level inside the wall box represents a zero water-pressure contour. These new
301 hydraulic boundary conditions are used for a steady-state water pressure calculation, following
302 Darcy's law. In the groundwater calculation, the water is considered incompressible. The newly
303 computed pore pressure field is used to evaluate excess pore pressure and corresponding out-of
304 balance forces that, during a plastic calculation stage, are applied stepwise into the finite element
305 mesh using the automatic load stepping procedures.
306
307 **3.1.5. Consideration of jet-grout treatments**
308 As previously explained, two different jet-grouting treatments were executed at the station, the
309 excavation bottom slab (Phase C, Table 1) and the columns adjacent to the diaphragm wall panels
310 (Phase E, Table 1).
311 In the model, the excavation jet-grouted bottom slab was considered undrained and its behavior
312 characterized with a simple linear elastic-perfectly plastic constitutive model. As the material
313 remains far from failure, the use of more advanced models (Arroyo et al. 2012) was deemed
314 unnecessary. Data from similar jet-grouting treatments in the same soil formations (Eramo et al.
315 2011) allowed estimating the parameters assigned to the bottom slab (Table 5). Such data indicate a
316 mean unconfined compressive strength (*UCS*) for jet-grout samples of approximately 3.5 MPa and a
317 ratio of the elastic modulus (*E*) to *UCS* equal to 700 on average. The lower bound value of *UCS*, on
318 the other hand, is around 800 kPa. Following Schnaid et al. (2001), the jet-grouting slab friction
319 angle is maintained equal to that of the original soil ($\varphi = 27.5^{\circ}$), while the effective cohesion is
320 increased to represent the bonding effect. Somewhat conservatively, cohesion is assigned a value (*c*

321 = 400 kPa) equal to half the lower bound of *UCS*, while the elastic modulus is selected close to the
322 estimated mean value (3.5 MPa · 700 ≈ 2500 MPa). The implications of these choices are later
323 explored.

324 In the numerical model, the jet-grouted bottom slab was simply wished-in-place. It was
325 recognized that, occasionally, installation of jet grouted slabs has caused movements in diaphragm
326 walls as well as in nearby buildings (Wong and Poh 2000). This possibility is later explored through
327 parametric analyses. As for the external jet-grout columns adjacent to the wall joints, little
328 information was available about the interface strength between jet injections and diaphragm walls.
329 Some authors (Obrzug and Preisig 2013) use tension-free interfaces. Ho et al. (2002) report very
330 low skin resistances in piles bored through jet-grout. The effects of both jet erosion and subsequent
331 retraction at set-up seem unfavorable for adherence. That is why, to reproduce the effect of these
332 columns in the model, the diaphragm wall stiffness was increased while its interface strength
333 reduced. PLAXIS allows doing so by means of a reduction factor, R_{inter}, which is applied to the
334 shear strength derived from the soil parameters of each unit. The value of R_{inter} at the diaphragm
335 wall-soil interface was set equal to 0.125 wherever the jet-grout columns are present and equal to
336 0.7 elsewhere, in line with conventional practice (Brinkgreve et al. 2008). Again, the consequences
337 of this choice are later examined through parametric analyses.

338

339 **3.2. Parametric analyses**

340 Three groups of parametric analyses were performed. A first group focuses on soil stiffness
341 parameters, a second one explores different model drainage hypotheses and a third one examines
342 alternative approaches to represent the effects of jet-grouting treatments. Outputs from these
343 analyses are presented in the following paragraphs, after the results of the Base Case are examined
344 in detail.

345

346 **4. Results**

4.1. Base Case

Figs. 6 and 7 show the comparison between numerical results and monitoring data referring respectively to the second dewatering stage (down to 18 m depth, Phase M) and the excavation to the deepest level (Phase N). All pictures refer to cumulative displacement results. In them, negative vertical displacements indicate settlements, while horizontal movements are negative in the direction of the excavation. Supplemental Data (Figs. S3 and S4) contain the results relative to the rest of construction stages.

Computed displacements follow satisfactorily all observed data (Figs. 6a-6d, 7a-7d, S3a-S3d and S4a-S4d). Computed pore pressures show a peak at the jet-grouted slab but the absence of measurements inside this layer does not allow confirming such response on site (Figs. 6f and S3f). In addition, there is some discrepancy with piezometric measurements at depth (Figs. 6e-6f and S3e-S3f). This is very likely attributable to smearing effects during piezometer installation.

At the final excavation stage (Fig. 7), the top of the diaphragm wall moves outwards (Fig. 7a). The model does catch this behavior and the extensometer measurements clearly illustrate that most vertical movements take place in the silty layers (below 10 m depth, Fig. 7b). At this stage, there is better agreement with the data in the near field (inclinometer and extensometer, Figs. 7a-7b) than with the observed building displacements (Figs. 7c-7d). Those are well captured on average, yet the different building sections show higher variability in the model than in the field.

4.2. Effect of stiffness soil parameters

Extra analyses were performed to examine the effect of both the power parameter *m* and the small strain modulus on the response of the constitutive model. The slope of oedometer and small strain shear moduli versus depth (Fig. 4) was used to estimate the *m* parameter. The noisy pattern of the data, due to the silty and sandy interlayers, made this evaluation difficult. For this reason, the *m*

parameter was varied from 0.5 to 1.0 in subsequent analyses. The effect of these changes on numerical results was very small (less than 3%).

A separate analysis focused on the effects of the HSSmall constitutive model versus the ones of the simpler Hardening Soil model (HS model, Schanz et al. 1999), which does not consider the non-linearity of soil stiffness at small strains. As expected, these new results (Fig. 8) show far larger movements than those resulting from the Base Case, significantly overestimating the observed data.

4.3. Effects of drainage hypothesis

As previously mentioned, in the Base Case the upper soil layers have drained behavior while the lower ones are undrained. There is little doubt about the drained behavior of the sand dominated layers (UG4 and above), where cone penetration is drained. The situation for the lower layers is not so clear due to the presence of more silty interbedded layers (Fig. 3). This issue was explored by performing two extra numerical analyses, a staged consolidation analysis in which all phases were timed according to the construction sequence reported in Table 1 (see Table 3 for the hydraulic conductivity values) and a fully drained analysis (Fig. S5 in the Supplemental Data).

The introduction of consolidation leads to a slightly less accurate prediction than the undrained simulation. This is likely a reflection of the uncertainty on hydraulic conductivity estimates. It is also possible that during on site construction very little consolidation took place in the lower soil layers. As expected, the fully drained response results in large settlement overestimations.

4.4. Effect of jet-grouting idealizations

As already pointed out, two different jet-grouting treatments were executed on site: the excavation base slab and a number of isolated columns behind the diaphragm wall joints. Additional numerical analyses helped exploring the numerical representation of both treatments.

For the case of the jet-grouted slab, installation and stiffness effects are examined. Installation effects are studied in the model by considering an initial phase in which a low stiffness slab is

activated and a small distributed volume expansion (0.5%) is assigned to all elements representing it. These hypotheses are based on the results of previous back-analyses relative to other jet-grouting treatments, as well as on the observation of increased void ratios on jet-grouted soils in the same area (Arroyo and Gens 2009). A separate analysis explores the effects of assigning a conservative value not just to the cohesion of the treated soil but also to its stiffness (E = 750 MPa). The volume expansion of jet-grout elements induces much higher wall displacement than observed data (Fig. 9). On the other hand, a reduced slab stiffness improves the comparison of numerical results with inclinometer observations, even though computed building settlements result larger than monitoring data (Fig. 9).

In order to study the jet-grout columns behind the diaphragm wall, interface strength and stiffening effects are analyzed. It has already been mentioned that the wall-soil interface might be characterized by a low strength value, hence the selection of R_{inter} = 0.125 for the Base Case (Case A). Additional analyses were run in order to explore the possibility of maintaining the standard R_{inter} value used for areas without jet-grout treatment (R_{inter} = 0.7). It is not clear from the results whether considering a reduced interface strength is appropriate. While wall movements are better captured with a reduced interface strength (Case A), computed building settlements are closer to the observed ones when no strength reduction is considered (Case C) (Fig. 10).

The presence of a stiffer reinforced soil close to the diaphragm wall may actually restrict wall deflections. Two different modeling options were explored to take into account the stiffening effect of the jet-grouted columns. In the first one, a row of soil elements adjacent to the wall is modeled as a material with an increased stiffness (E = 1000 MPa). The second option, on the other hand, considers an increased width of the plate elements (from 1.2 m to 2.5 m) assuming a composite section for the wall.

Table 6 presents the different cases considered in the numerical analyses. Fig. 10 illustrates the effect of these modeling options both on wall displacements and on building settlements after the

423 last excavation stage. It is clear that the composite-section approach better represents the stiffening
424 effect of the jet-grout injections. In this case, in fact, numerical results are closer to observed data.
425
426 **5. Conclusions**
427 The present work demonstrates that it is possible to obtain a good representation of the behavior
428 of deep excavations with the use of finite element models in which most parameters are obtained
429 from dilatometer tests (DMT and SDMT). In this case study, a thick layer of soft soil made
430 characterization based on laboratory testing very difficult. SDMT offered a good alternative to
431 estimate the dependence of soil stiffness on stress/strain level, which is crucial for accurate
432 modeling.
433 The numerical results based on the estimated data adequately reproduce all monitoring
434 measurements in most phases of the construction process. The dilatometer test proves therefore
435 appropriate to provide representative parameters for a range of soil materials with different
436 permeability and drainage conditions. Analyses also show the importance of considering high soil
437 stiffness values in the small strain range. In this respect, the direct determination of small strain
438 moduli by SDMT represents a clear advantage.
439 However, even when good-quality site investigation data is available, uncertainties do invariably
440 remain. In the present case study, significant uncertainties were associated with the modeling of jet-
441 grouting treatments undertaken both to form the bottom slab of the excavation and to seal the
442 potential gaps between diaphragm wall panels. A parametric study was hence performed to explore
443 the effects of different modeling options. The study indicates the need for further research on the
444 effects of jet-grouting installation as well as on the outcomes of jet injections on soil-structure
445 interfaces. Notwithstanding these difficulties, the work presented provides strong evidence for the
446 possibility of achieving adequate models of deep excavations in soft soil whenever soil parameters
447 are obtained from well-conducted in-situ dilatometer tests.
448

Acknowledgements

This research was partly supported by the Spanish Ministry of Economy through grant (BIA2014-59467-R).

Supplemental Data

Table S1, Figs. S1-S5 are available on line in the ASCE Library (www.ascelibrary.org).

References

Amoroso, S., Lehane, B., and Fahey, M. (2013). "G-γ decay curves in sand by Seismic Dilatometer (SDMT)." *Proc., 4th Int. Conf. on Geotechnical and Geophysical Site Characterization*, Taylor & Francis Group, London, 447-452.

Amoroso, S., Monaco, P., Lehane, B.M., and Marchetti D. (2014). "Examination of the potential of the seismic dilatometer (SDMT) to estimate in situ stiffness decay curves in various soil types." *Soils and Rocks*, 37(3), 177-194.

Arroyo, M., Ciantia, M., Castellanza, R., Gens, A., and Nova, R. (2012). "Simulation of cement-improved clay structures with a bonded elasto-plastic model: a practical approach." *Computers and Geotechnics*, 45, 140-150.

Arroyo, M., Di Mariano, A., Gens, A., Alonso, E., García Fontanet, A., and García Germán, J. (2007). "Management of third-party risk in an urban deep excavation project." *Proc., 14th Eur. Conf. of Soil Mech. and Geotech. Eng.*, Millpress, Rotterdam, 527-532.

Arroyo, M., Di Mariano, A., Monaco, P., Devincenzi, M., and Pérez, N. (2008). "SDMT-based deep excavation design." *Proc., 3rd Int. Conf. on Site Characterization*, Taylor & Francis Group, London, 967-973.

Arroyo, M., and Gens, A. (2009). "Engineering assessment of jet-grouted structures." *Proc., 17th Int. Conf. on Soil Mech. and Geotech. Eng.*, IOS Press, Amsterdam, 2338-2341.

474 Arroyo, M., and Mateos, T. (2006). "Embankment design with DMT and CPTu: prediction and
475 performance." *Proc., 2nd Int. Flat Dilatometer Conf.*, R.A. Failmezger and J.B. Anderson (eds),
476 In-Situ Soil Testing, Lancaster, VA, 62-68.
477 Arroyo, M., Mateos, T., Devincenzi, M., Gómez-Escoubes, R., and Martínez, J.M. (2004). "CPTu-
478 DMT performance-based correlation for settlement design." *Proc., 2nd Int. Conf. on Site*
479 *Characterization*, Millpress, Rotterdam, 1605-1610.
480 Been, K., Quiñonez, A., and Sancio, R.B. (2010). "Interpretation of the CPT in engineering
481 practice." *Proc., 2nd Int. Symp. on Cone Penetration Testing*, Omnipress, Madison, WI.
482 Benz, T. (2007). "Small-Strain Stiffness of Soils and its Numerical Consequences." Ph.D. thesis,
483 Universität Stuttgart.
484 Bosco, G., and Monaco, P. (2016). "Strain moduli of alluvial soils from CPT, DMT, Vs, and lab
485 tests." *Proc., 5th Int. Conf. on Geotechnical and Geophysical Site Characterization*, Australian
486 Geomechanics Society, Sydney, 395-400.
487 Brinkgreve, R.B.J., Bakker, K.J., and Bonnier, P.G. (2006). "The relevance of small-strain soil
488 stiffness in numerical simulation of excavation and tunnelling projects." *Numerical Methods in*
489 *Geotechnical Engineering*, CRC Press, Taylor & Francis Group, London, 133-139.
490 Brinkgreve, R.B.J., Broere, W., and Waterman D. (2008). *Plaxis 2D Version 9.0*.
491 Burland, J.B. (1989). "Small is beautiful – the stiffness of soils at small strains." *Canad. Geotech.*
492 *J.*, 26(4), 499-516.
493 Calvello, M., and Finno, R.J. (2004). "Selecting parameters to optimize in model calibration by
494 inverse analysis." *Computers and Geotechnics*, 31(5), 410-424.
495 Cho, W., and Finno, R.J. (2009). "Stress-strain responses of block samples of compressible Chicago
496 glacial clays." *J. Geotech. Geoenviron. Eng.*, 136(1), 178-188, 10.1061/(ASCE)GT.1943-
497 5606.0000186.

498 Cox, C., and Mayne, P.W. (2015). "Soil stiffness constitutive model parameters for geotechnical
499 problems: A dilatometer testing approach." *Proc., 3rd Int. Conf. on Flat Dilatometer*, S.
500 Marchetti et al. (eds), Rome, 393-400.
501 Dias, T.G.S., and Bezuijen, A. (2013). "General report of TC204: underground constructions."
502 *Proc., 18th Int. Conf. on Soil Mech. and Geotech. Eng.*, Presses des Ponts, Paris, 1673-1680.
503 Di Mariano, A., Gesto, J.M., Gens, A., and Schwarz, H. (2007). "Ground deformation and
504 mitigating measures associated with the excavation of a new Metro line." *Proc., 14th Eur. Conf.*
505 *of Soil Mech. and Geotech. Eng.*, Millpress, Rotterdam, 1901-1906.
506 Eramo, N., Modoni, G., and Arroyo, M. (2011). "Design control and monitoring of a jet grouted
507 excavation bottom plug." *Proc., 7th Int. Symp. on Geotechnical Aspects of Underground*
508 *Construction in Soft Ground*, CRC Press, Taylor & Francis Group, London, 611-618.
509 Fahey, M., and Carter, J.P. (1993). "A finite element study of the pressuremeter test in sand using a
510 non-linear elastic plastic model." *Canad. Geotech. J.*, 30(2), 348-362.
511 Finno, R.J. (2010). "Evaluating Excavation Support Systems to Protect Adjacent Structures." *DFI*
512 *Journal – The Journal of the Deep Foundations Institute*, 4(2), 3-19.
513 Gámez, D. (2007). "Sequence Stratigraphy as a tool for water resources management in alluvial
514 coastal aquifers: application to the Llobregat delta (Barcelona, Spain)." PhD thesis, Universitat
515 Politècnica de Catalunya.
516 Garitte, B., Arroyo, M., and Gens, A. (2010). "Analysis of ground movements induced by
517 diaphragm wall installation." *Proc., 7th Eur. Conf. on Numerical Methods in Geotechnical*
518 *Engineering*, CRC Press, Taylor & Francis Group, London, 547-552.
519 Gens, A., Di Mariano, A., Gesto, J.M., and Schwarz, H. (2006). "Ground movement control in the
520 construction of a new metro line in Barcelona." *Proc., Geotechnical Aspects of Underground*
521 *Construction in Soft Ground*, Taylor & Francis Group, London, 389-395.

522 Gens, A., Di Mariano, A., and Yubero, M.T. (2011). "EPB tunnelling in deltaic deposits:
523 observations of ground movements." *Proc., Geotechnical Aspects of Underground Construction*
524 *in Soft Ground*, Taylor & Francis Group, London, 987-993.
525 Gens, A., and Lloret, L. (2003). "Monitoring a preload test on soft ground." Field Measurements in
526 Geomechanics, *Proc., 6th Int. Symp. FMGM 2003*, Swets & Zeitlinger B.V., Lisse, The
527 Netherlands, 53-59.
528 Hashash, Y.M., Marulanda, C., Ghaboussi, J., and Jung, S. (2006). "Novel approach to integration
529 of numerical modeling and field observations for deep excavations." *J. Geotech. Geoenviron.*
530 *Eng.*, 132(8), 1019-1031, 10.1061/(ASCE)1090-0241(2006)132:8(1019).
531 Hashash, Y.M., and Whittle, A.J. (1996). "Ground movement prediction for deep excavations in
532 soft clay." *J. Geotech. Eng.*, 122(6), 474-486, 10.1061/(ASCE)0733-9410(1996)122:6(474).
533 Ho, C.E., Lim, C.H., and Tan, C.G. (2002). "Characteristics of bored piles installed through jet
534 grout layer." *J. Performance of Constructed Facilities*, 16(4), 160-168.
535 Jardine, R.J. (1992). "Nonlinear stiffness parameters from undrained pressuremeter tests." *Canad.*
536 *Geotech. J.*, 29(3), 436-447.
537 Jardine, R.J., Standing, J.R., and Kovacecic, N. (2005). "Lessons learned from full scale
538 observations and the practical application of advanced testing and modeling." *Deformation*
539 *Characteristics of Geomaterials*, Taylor & Francis Group, London, 201-245.
540 Khoiri, M., and Ou, C.Y. (2013). "Evaluation of deformation parameter for deep excavation in sand
541 through case histories." *Computers and Geotechnics*, 47, 57-67.
542 Ledesma, A., Gens, A., and Alonso, E.E. (1996). "Estimation of parameters in geotechnical
543 backanalysis – I. Maximum likelihood approach." *Computers and Geotechnics*, 18(1), 1-27.
544 Lehane, B.M., and Fahey, M. (2004). "Using SCPT and DMT data for settlement prediction in
545 sand." *Proc., 2nd Int. Conf. on Site Characterization*, Millpress, Rotterdam, 1673-1679.
546 Marchetti, S. (1980). "In situ tests by flat dilatometer." *J. Geotech. Engrg. Div.*, 106(3), 299-321.

547 Marchetti, S. (1997). "The Flat Dilatometer: Design Applications." *Proc., 3rd Int. Geotechnical*
548 *Engineering Conf.,* Cairo University, 421-448.
549 Marchetti, S., and Crapps, D. K. (1981). "Flat dilatometer manual." G.P.E. Inc., Gainesville, FL.
550 Marchetti, S., Monaco, P., Totani, G., and Marchetti, D. (2008). "In Situ Tests by Seismic
551 Dilatometer (SDMT)." *From Research to Practice in Geotechnical Engineering*, *Geotech. Spec.*
552 *Pub. No. 180,* 292-311, 10.1061/40962(325)7.
553 Mayne, P.W., Schneider, J.A., and Martin, G.K. (1999). "Small- and large-strain soil properties
554 from seismic flat dilatometer tests." *Pre-failure Deformation Characteristics in Geomaterials*,
555 Balkema, Rotterdam, 419-427.
556 Monaco, P., Amoroso, S., Marchetti, S., Marchetti, D., Totani, G., Cola, S., and Simonini, P.
557 (2014). "Overconsolidation and Stiffness of Venice Lagoon Sands and Silts from SDMT and
558 CPTU." *J. Geotech. Geoenviron. Eng.*, 140(1), 215-227, 10.1061/(ASCE)GT.1943-
559 5606.0000965.
560 Monaco, P., and Marchetti, S. (2004). "Evaluation of the coefficient of subgrade reaction for design
561 of multipropped diaphragm walls from DMT moduli." *Proc., 2nd Int. Conf. on Site*
562 *Characterization*, Millpress, Rotterdam, 993-1002.
563 Monaco, P., Totani, G., and Calabrese, M. (2007). "DMT-predicted vs observed settlements: a
564 review of the available experience." *Studia Geotechnica et Mechanica*, XXIX(1-2), 103-120.
565 Obrzug, R., and Preisig, M. (2013). "Large scale 3D numerical simulations of deep excavations in
566 urban areas–constitutive aspects and optimization." *Mitteilungen der Geotechnik Schweiz*, 167,
567 57-68.
568 Ou, C.Y. (2016). "Finite element analysis of deep excavation problems." *Journal of*
569 *GeoEngineering*, 11(1), 1-12.
570 Pepe, G., Coen, G., Napoleoni, Q., Pagliaroli, A., Stigliano, F., Mancini, M., Lanzo, G., Silvani,S.,
571 Scarapazzi, M., and Storoni Ridolfi, S. (2015). "SDMT Testing for the Estimation of In Situ G-γ

572 Decay Curves in Soft Alluvial and Organic Soils." *Proc., 3rd Int. Conf. on Flat Dilatometer*, S.
573 Marchetti et al. (eds), Rome, 423-430.
574 Pineda, J.A., Arroyo, M., Sau, N., Gens, A., and Pérez, N. (2012). "Testing block samples from
575 silty deposits." *Proc., 4th Int. Conf. on Site Characterization*, Taylor & Francis Group, London,
576 1815-1823.
577 Rodrigues, C., Amoroso, S., Cruz, N., and Cruz, J. (2016). "*G*-γ decay curves in granitic residual
578 soils by seismic dilatometer." *Proc., 5th Int. Conf. on Geotechnical and Geophysical Site*
579 *Characterization*, Australian Geomechanics Society, Sydney, 1137-1142.
580 Sau, N., Arroyo, M., and Gens, A. (2012). "Site characterization alternatives for numerical models
581 of a deep excavation." *Proc., 4th Int. Conf. on Site Characterization*, Taylor & Francis Group,
582 London, 1169-1177.
583 Schanz, T., Vermeer, P.A., and Bonnier, P.G. (1999). "The hardening soil model: formulation and
584 verification." *Beyond 2000 in Computational Geotechnics – 10 Years of PLAXIS*, Balkema,
585 Rotterdam, 1-16.
586 Schnaid, F., Prietto, P.D., and Consoli, N.C. (2001). "Characterization of cemented sand in triaxial
587 compression." *J. Geotech. Geoenviron. Eng.*, 127(10), 857-868, 10.1061/(ASCE)1090-
588 0241(2001)127:10(857).
589 St John, H.D., Potts, D.M., Jardine, R.J., and Higgins, K.G. (1993). "Prediction and performance of
590 ground response due to construction of a deep basement at 60 Victoria Embankment." *Predictive*
591 *Soil Mechanics*, Thomas Telford, London, 581-608.
592 Vermeer, P.A. (2001). "On single anchored retaining walls." *Plaxis Bulletin* 10.
593 Wong, I.H., and Poh, T.Y. (2000). "Effects of jet grouting on adjacent ground and structures." *J.*
594 *Geotech. Geoenviron. Eng.*, 126(3), 247-256, 10.1061/(ASCE)1090-0241(2000)126:3(247).
595 Yoo, C., Park, S.W., Kim, B., and Ban, H. (eds) (2014). "Geotechnical aspects of underground
596 construction in soft ground." CRC Press, Taylor & Francis Group, London.
597

598 **List of figures & captions**

599

600 **Fig. 1.** Plan of the Verge de Montserrat Station and location of in situ tests

601 **Fig. 2.** Cross section A_A' with a schematic representation of the 6-storey building

602 **Fig. 3.** Profiles of soil parameters from all DMT/SDMT and CPTu tests

603 **Fig. 4.** Comparison between the profiles of E_{oed} (a) and G_0 (b) obtained from DMT/SDMT and
604 adopted in the FEM analysis

605 **Fig. 5.** Normalized stiffness decay curves G/G_0-γ estimated from SDMT for each geotechnical unit
606 with intersection points (black dots) corresponding to the shear moduli 0.722 G_0 and to the shear
607 strains $\gamma_{0.7}$

608 **Fig. 6.** Dewatering to 18 m depth (phase M): (a) diaphragm wall horizontal movements; (b)
609 diaphragm wall vertical movements; (c) six-storey building vertical movements; (d) six-storey
610 building horizontal movements; (e) pore pressure distribution outside the excavation and (f) pore
611 pressure distribution inside the excavation

612 **Fig. 7.** Excavation to deepest level (phase N): (a) diaphragm wall horizontal movements; (b)
613 diaphragm wall vertical movements; (c) six-storey building vertical movements; (d) six-storey
614 building horizontal movements

615 **Fig. 8.** Effect of the constitutive model on the comparison between measurements and simulation
616 results: (a) retaining wall movements computed with HSS; (b) retaining wall movement computed
617 with HS; (c) building settlements computed with HSS; (d) building settlements computed with HS

618 **Fig. 9.** Effect of hypotheses about jet-grouted slab: (a) on diaphragm wall movement at maximum
619 excavation (phase N); (b) on building settlement at maximum excavation (phase N)

620 **Fig. 10.** Effect of hypotheses about jet-grout columns: (a) on diaphragm wall movement at
621 maximum excavation (phase N); (b) on building settlement at maximum excavation (phase N)

622 **Tables**

623

624

625 **Table 1.** Construction activities for the excavation of Verge de Montserrat Station

Phase	Activity	Start	End
A	Diaphragm walling	15 July 2009	06 August 2009
B	Construction of jet-grouting columns behind vertical joints among wall panels	16 September 2009	01 October 2009
C	Construction of bottom jet-grout slab	19 October 2009	01 December 2009
D	EPB tunnel excavation	02 December 2009	05 December 2009
E	Construction of extra jet-grouting columns behind the diaphragm walls adjacent to joints	09 December 2009	23 December 2009
F	Execution of tie beams	14 January 2010	29 January 2010
G	Excavation to main roof concrete slab level (2.5 m depth)	02 February 2010	16 February 2010
H	Construction of main roof concrete slab	25 February 2010	04 March 2010
I	1st dewatering down to a depth of 10 m	12 March 2010	01 April 2010
K	Excavation to 2nd concrete slab level (7.5 m depth)	30 March 2010	14 April 2010
L	Construction of 2nd concrete slab	21 April 2010	12 May 2010
M	2nd dewatering down to a depth of 18 m	03 June 2010	22 June 2010
N	Excavation to deepest level (18.5 m depth)	23 June 2010	27 October 2010
O	Construction of bottom concrete slab	25 August 2010	08 November 2010

626

627

628 **Table 2.** Characteristics of the structural elements

Structural element	EA (kN/m)	EI (kN/m^2/m)	d (m)	υ (-)	w (kN/m/m)
Retaining wall	$3.26 \cdot 10^7$	$3.92 \cdot 10^6$	1.20	0.15	7.86
Roof slab	$3.43 \cdot 10^7$	$4.11 \cdot 10^6$	1.20	0.20	30.00
Second slab	$2.18 \cdot 10^7$	$1.16 \cdot 10^6$	0.80	0.20	23.90
Tunnel lining	$1.40 \cdot 10^7$	$1.19 \cdot 10^5$	0.32	0.10	7.68
Building foundation slab	$2.00 \cdot 10^7$	$8.20 \cdot 10^5$	0.70	0.15	17.50

629

630

631 **Table 3.** HSSmall parameters for natural soil layers

UG	K (m/day)	γ (kN/m^3)	K_0^{nc} (-)	υ (-)	c (kN/m^2)	φ (°)	m (-)	E_{oed}^{ref} (MPa)	E_{50}^{ref} (MPa)	E_{ur}^{ref} (MPa)	G_0^{ref} (MPa)	$\gamma_{0.7}$ (-)
UG1	0.050	19.50	0.56	0.2	1.0	29.0	0.6	48.26	48.26	193.04	144.37	$3.4\cdot10^{-4}$
UG2	0.200	21.30	0.47	0.2	1.0	32.0	0.5	70.95	70.95	283.81	138.97	$7.0\cdot10^{-5}$
UG3	0.200	21.30	0.50	0.2	1.0	32.0	0.5	27.21	27.21	108.84	111.73	$3.2\cdot10^{-5}$
UG4	0.030	18.80	0.57	0.2	1.0	27.5	0.7	31.00	31.00	124.00	75.06	$4.2\cdot10^{-4}$
UG5	0.003	18.80	0.56	0.2	1.0	27.0	0.7	12.93	12.93	51.72	81.90	$1.6\cdot10^{-4}$
UG6	0.003	19.00	0.54	0.2	0.2	28.0	0.7	12.62	12.62	50.48	94.62	$1.4\cdot10^{-4}$
UG7	0.003	14.70	0.55	0.2	1.0	27.5	0.8	5.92	5.92	23.68	98.20	$6.5\cdot10^{-5}$
UG8	0.003	19.00	0.55	0.2	0.2	28.0	0.7	19.07	19.07	76.28	147.65	$1.3\cdot10^{-4}$

632

633

634 **Table 1.** Elasto-plastic (Mohr-Coulomb) parameters for fill layer

UG	γ (kN/m^3)	E (MPa)	υ (-)	c (kN/m^2)	φ (°)
R	17.5	10	0.3	0.1	26.0

635

636

637 **Table 2.** Elasto-plastic (Mohr-Coulomb) parameters for jet-grout slab

UG	γ (kN/m^3)	E (MPa)	υ (-)	c (kN/m^2)	φ (°)
JG	21.5	2500	0.3	400	27.5

638

639

640 **Table 3.** Alternative idealizations of jet-grout wall joint columns

CASE	Stiffening effect	Interface strength
A (Reference)	Wall section increase	Reduced
B	Jet elements	Reduced
C	Wall section increase	Standard
D	Jet elements	Standard

641

642

Figure 1

Click here to download Figure Fig. 1.tif

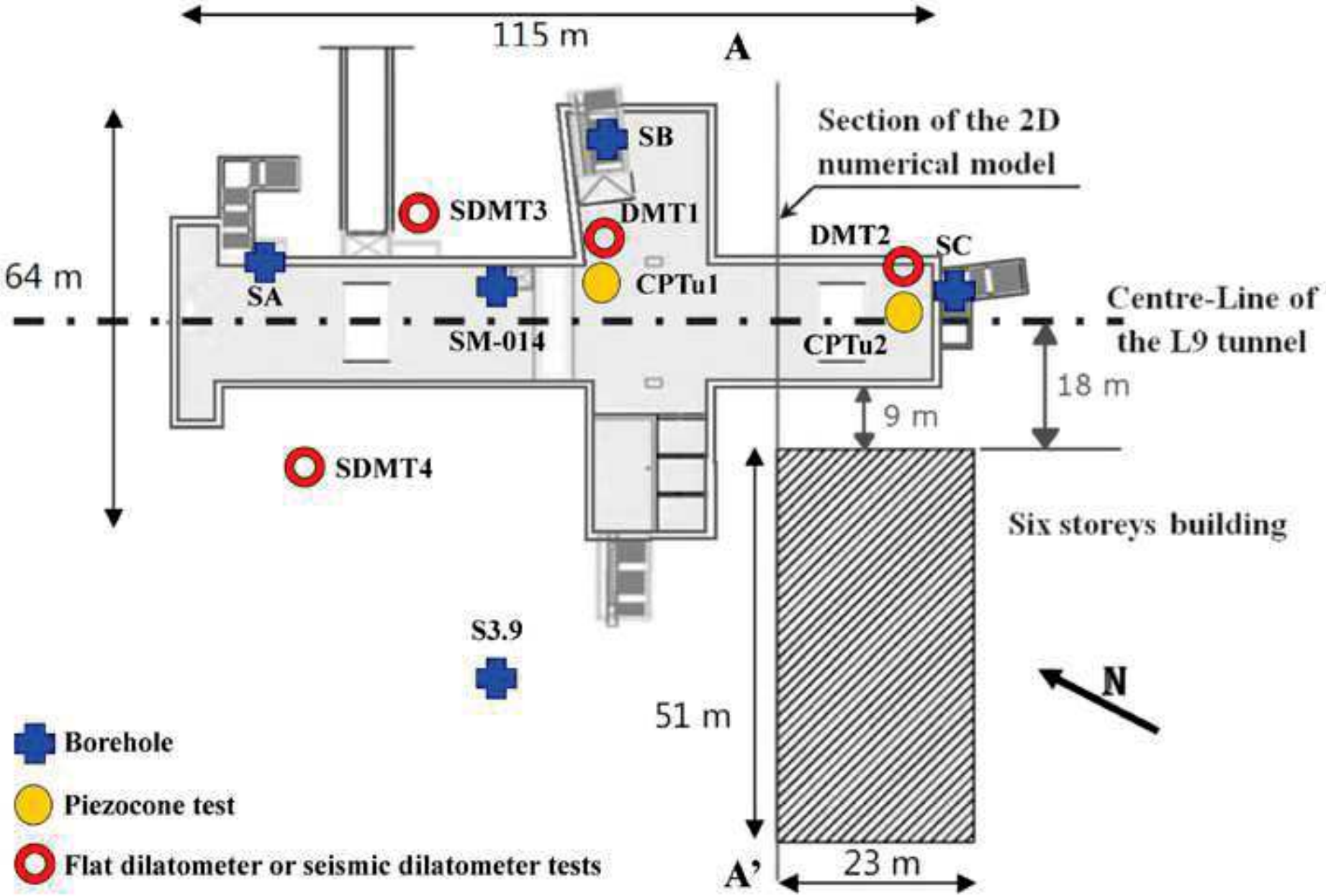

Figure 2

Click here to download Figure Fig. 2.tif

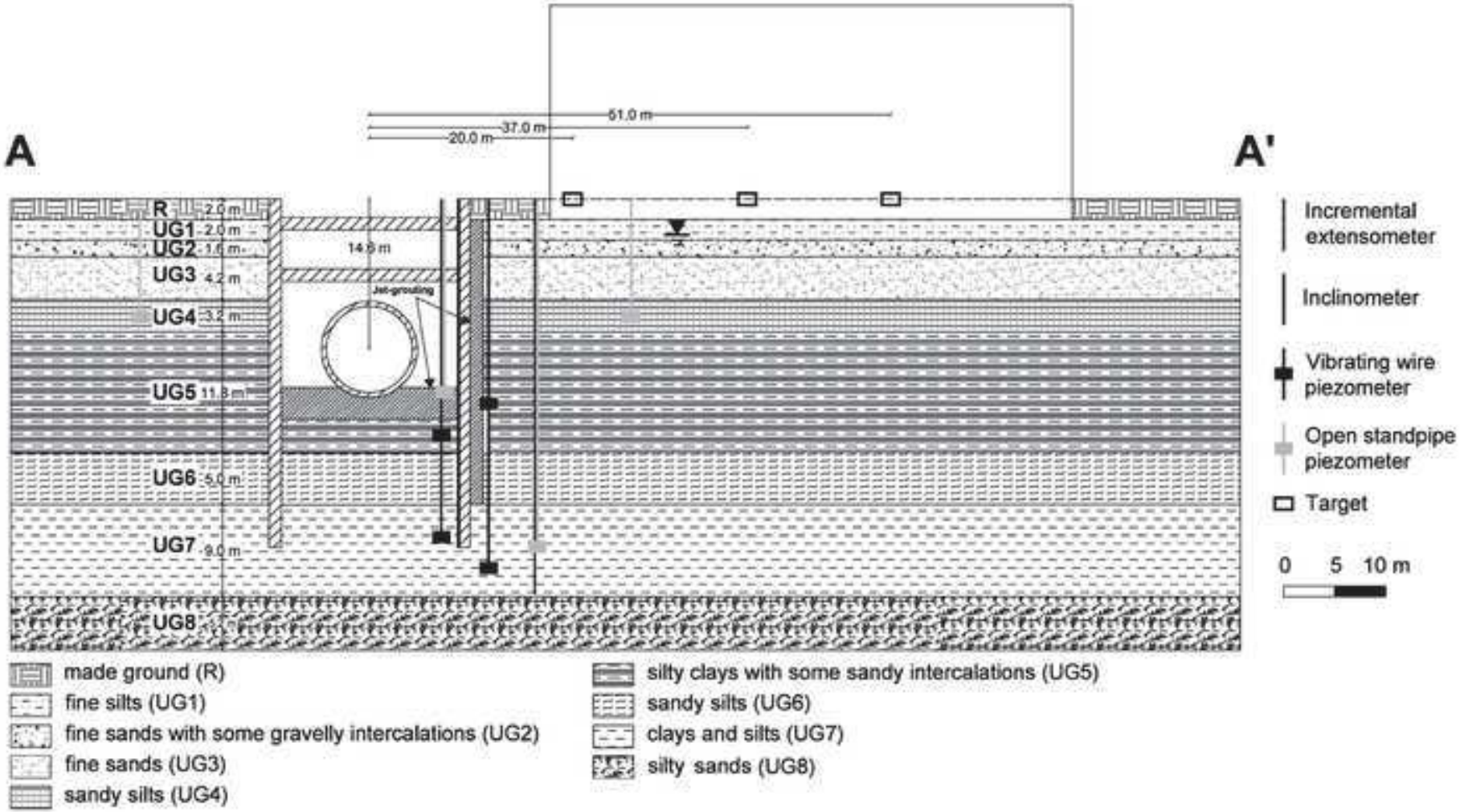

Figure 3

Click here to download Figure Fig. 3.tif

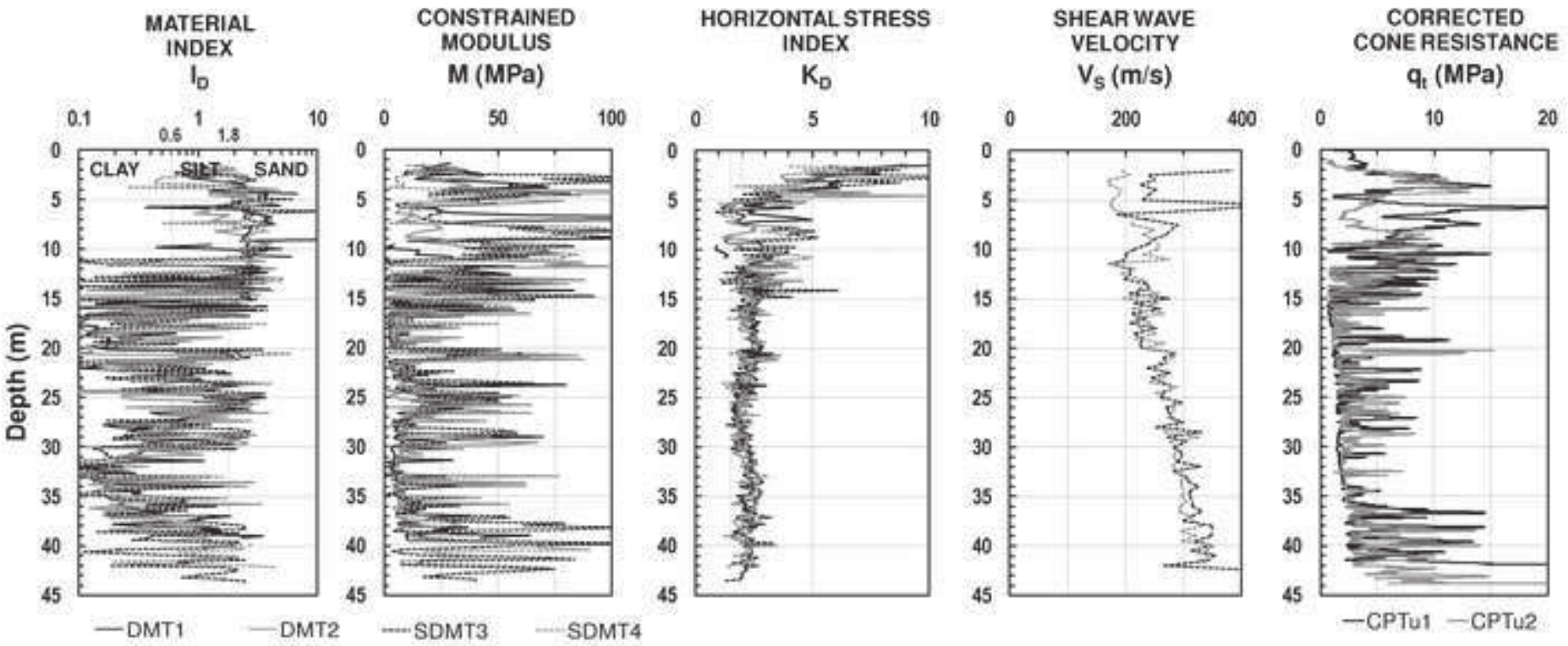

Figure 4

Click here to download Figure Fig. 4.tif

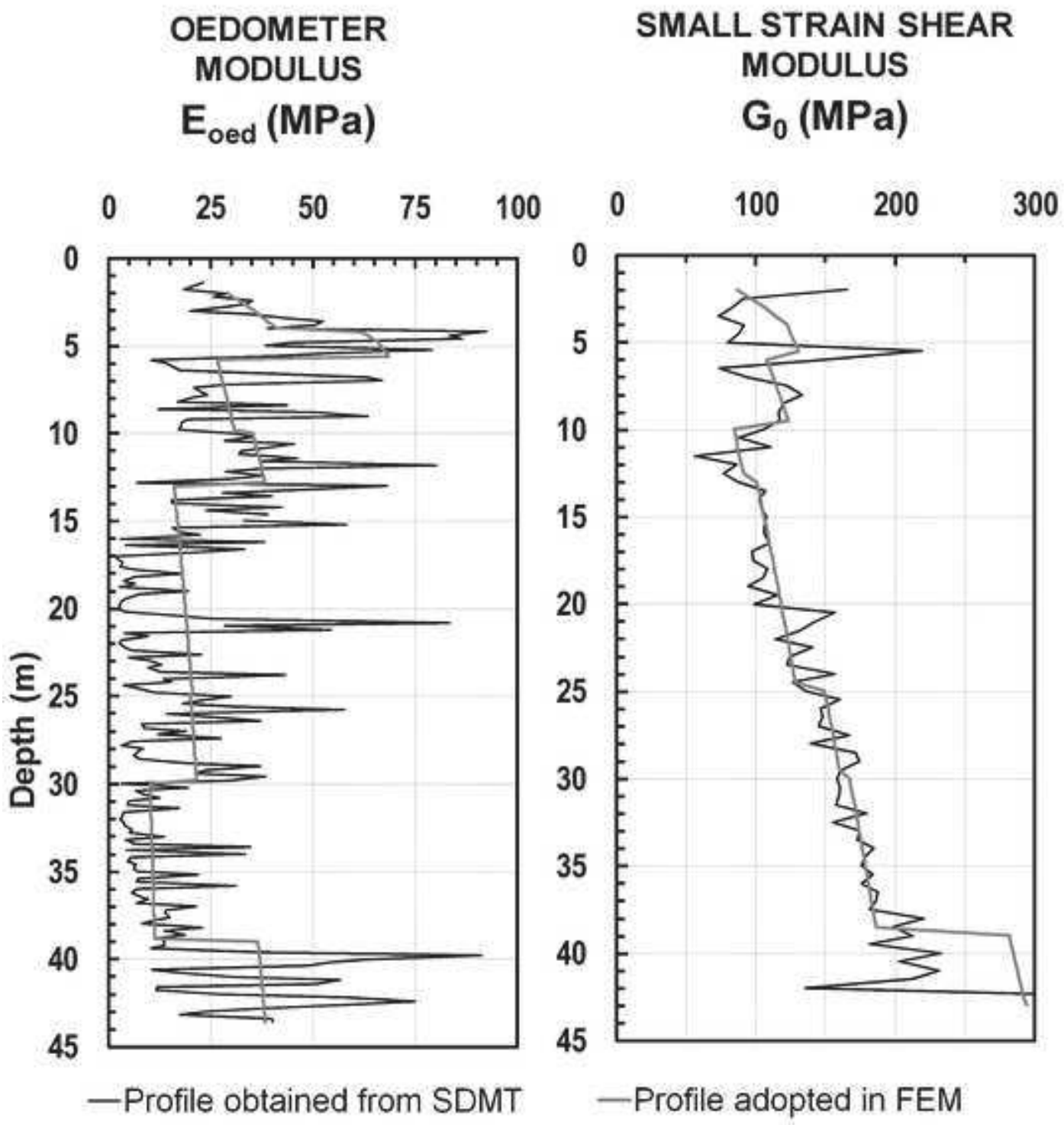

Figure 5

Click here to download Figure Fig. 5.tif

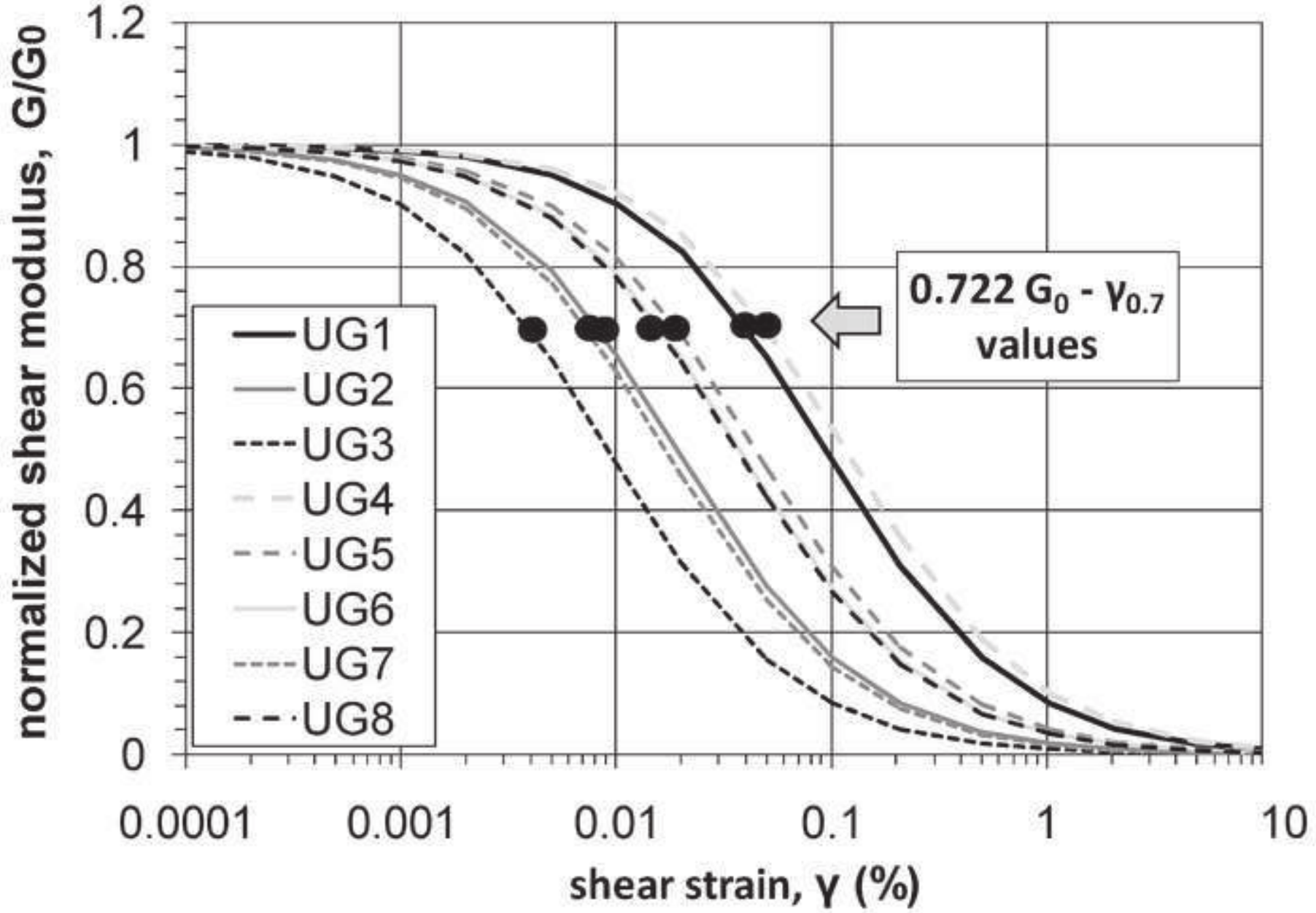

Figure 6

Click here to download Figure Fig. 6.tif

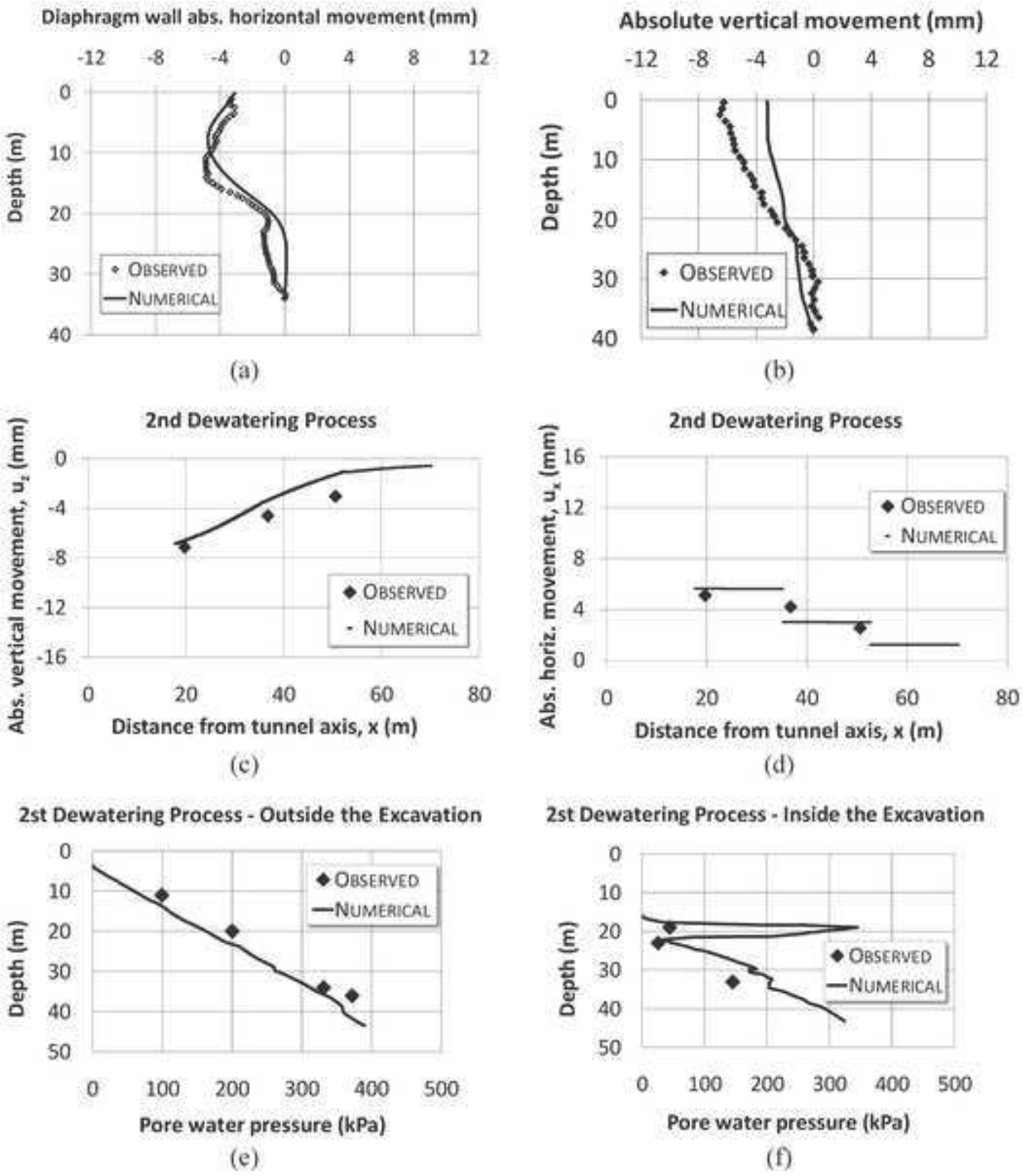

Figure 7

Click here to download Figure Fig. 7.tif

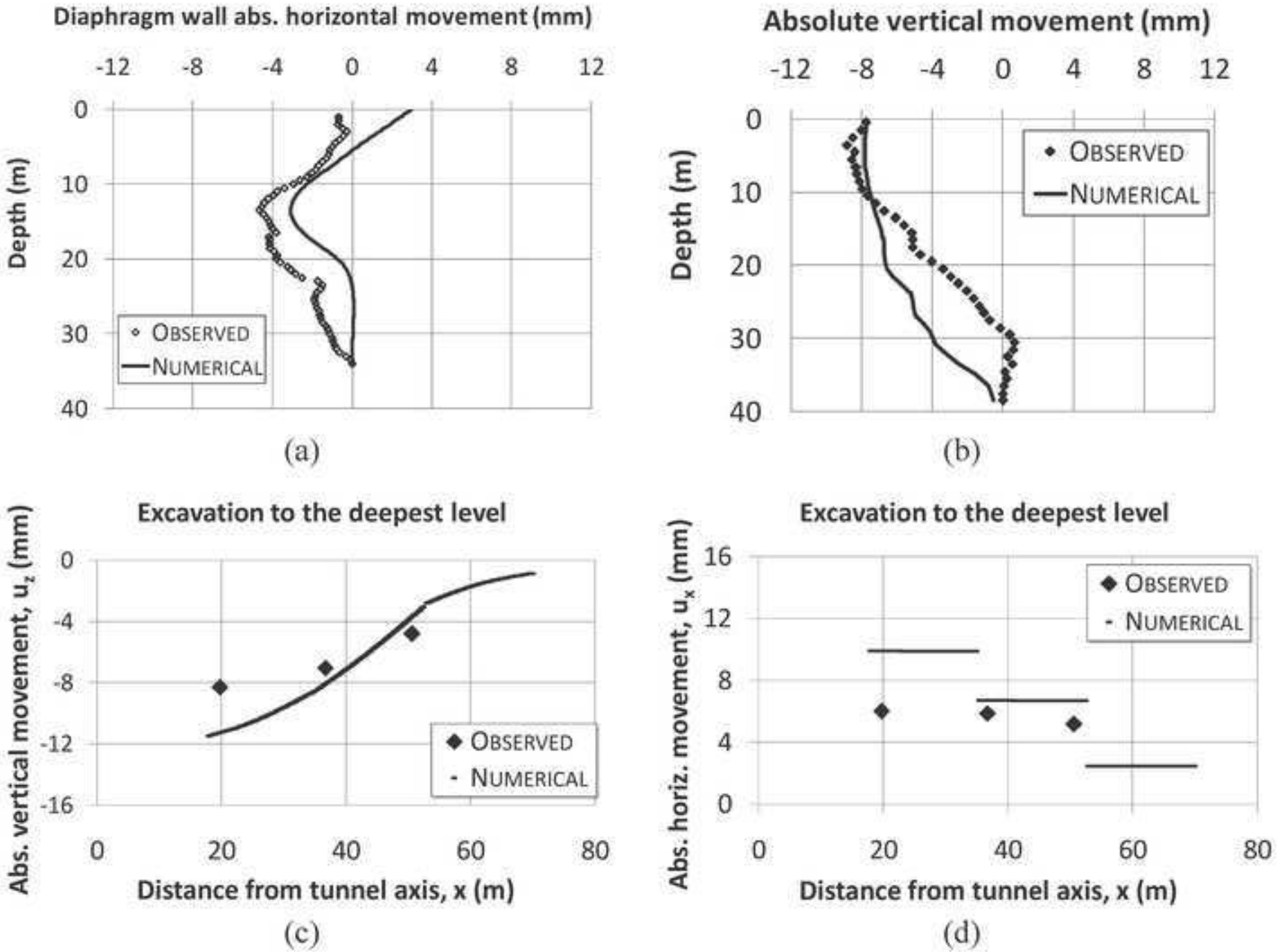

Figure 8

Click here to download Figure Fig. 8.tif

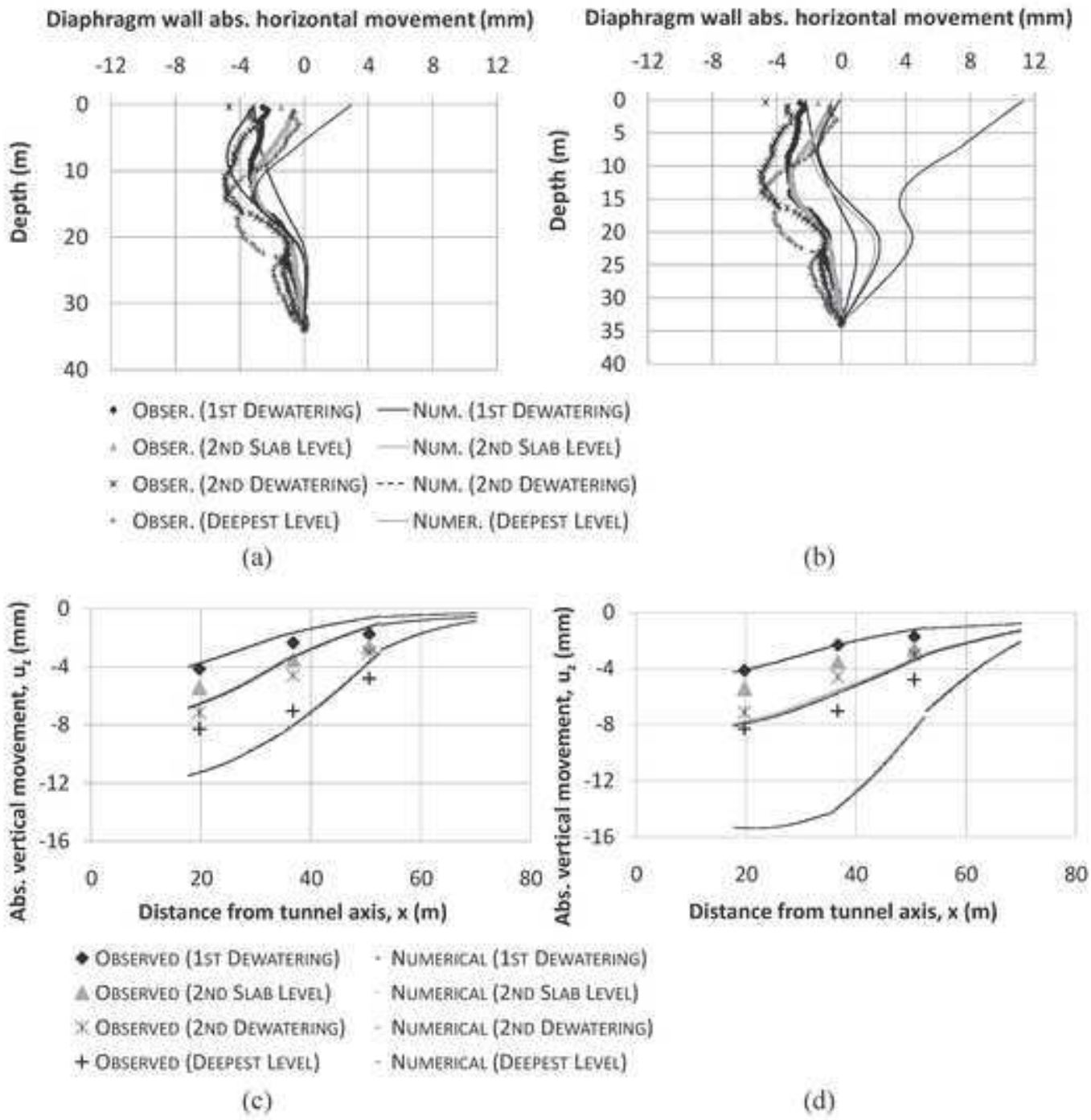

Figure 9

Click here to download Figure Fig. 9.tif

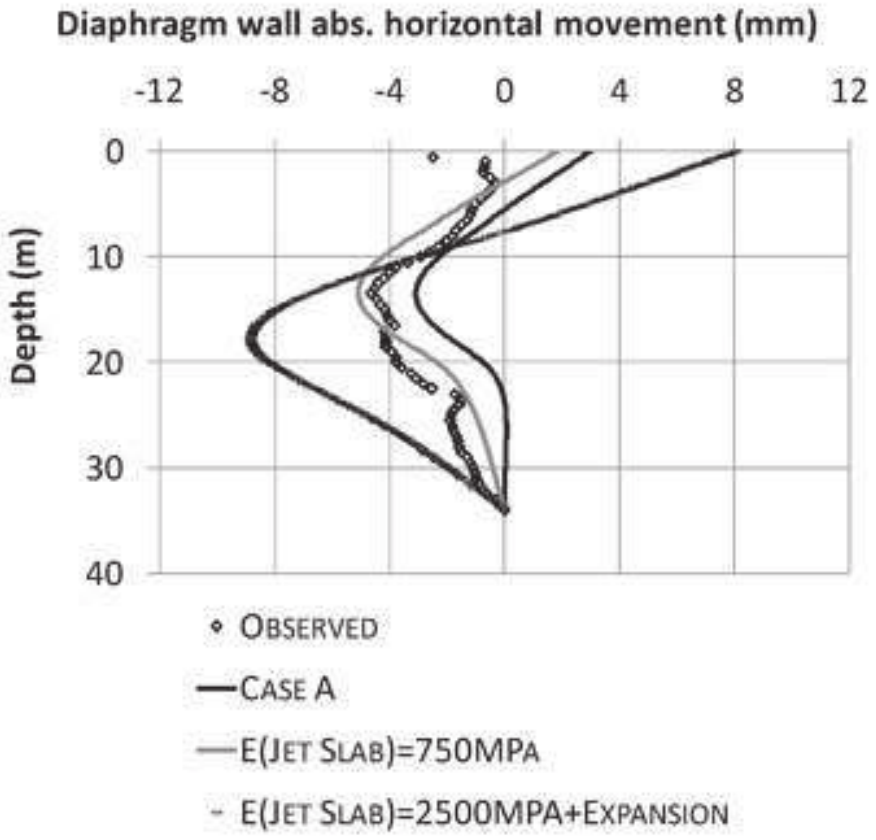

(a)

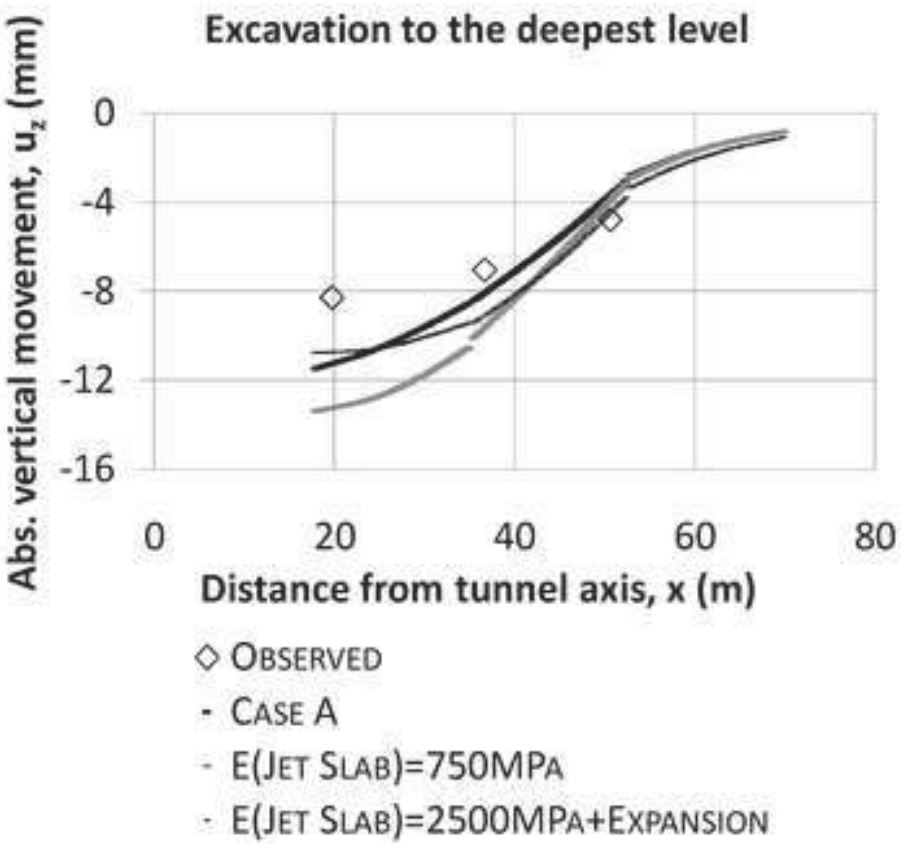

(b)

Figure 10

Click here to download Figure Fig. 10.tif

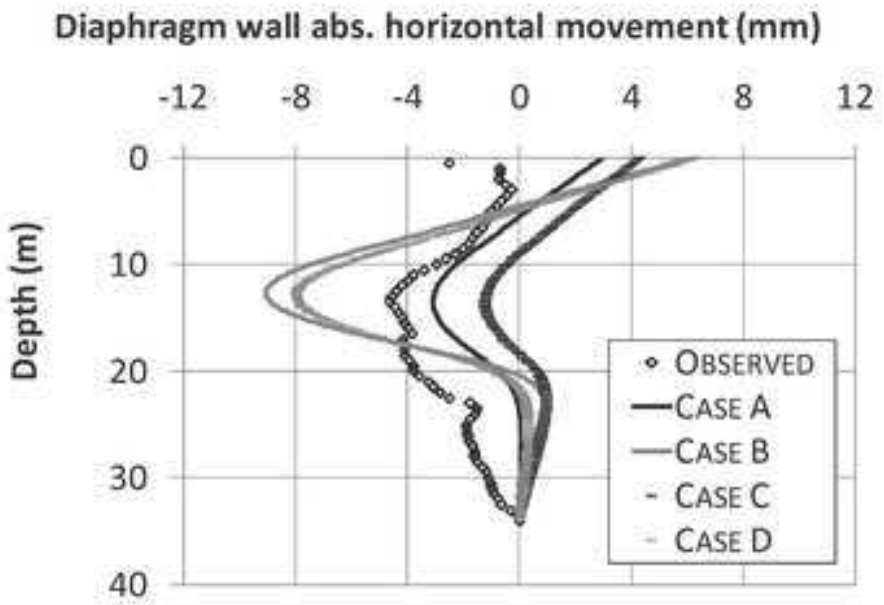

(a)

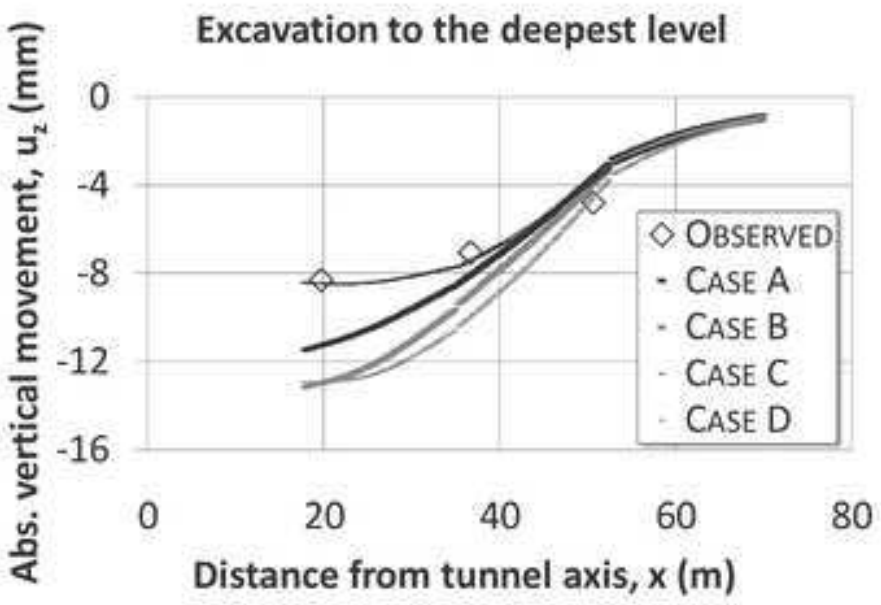

(b)

ASCE Authorship, Originality, and Copyright Transfer Agreement

Publication Title: Journal of Geotechnical and Geoenvironmental Engineering

Manuscript Title: Case Study: SDMT-based numerical analyses of a deep excavation in soft soil

Author(s) – **Names, postal addresses, and e-mail addresses of all authors**

Alessandra Di Mariano, Staff Scientist, International Center for Numerical Methods in Engineering (CIMNE), Barcelona, Spain, alessandra.dimariano@upc.edu

Sara Amoroso, Researcher, Istituto Nazionale di Geofisica e Vulcanologia, L'Aquila, Italy, sara.amoroso@ingv.it

Marcos Arroyo, Professor, Dept. of Civil and Environmental Engineering, Geosciences Division, Universitat Politècnica de Catalunya (UPC), Barcelona, Spain, marcos.arroyo@upc.edu

Paola Monaco, Assistant Professor, Dept. of Civil, Architectural and Environmental Engineering, University of L'Aquila, L'Aquila, Italy, paola.monaco@univaq.it

Antonio Gens, Professor, Dept. of Civil and Environmental Engineering, Geosciences Division, Universitat Politècnica de Catalunya (UPC), Barcelona, Spain, antonio.gens@upc.edu

I. Authorship Responsibility

To protect the integrity of authorship, only people who have significantly contributed to the research or project and manuscript preparation shall be listed as coauthors. The corresponding author attests to the fact that anyone named as a coauthor has seen the final version of the manuscript and has agreed to its submission for publication. Deceased persons who meet the criteria for coauthorship shall be included, with a footnote reporting date of death. No fictitious name shall be given as an author or coauthor. An author who submits a manuscript for publication accepts responsibility for having properly included all, and only, qualified coauthors.

I, the corresponding author, confirm that the authors listed on the manuscript are aware of their authorship status and qualify to be authors on the manuscript according to the guidelines above.

SARA AMOROSO	Sara Amoroso	11/09/2017
Print Name	Signature	Date

II. Originality of Content

ASCE respects the copyright ownership of other publishers. ASCE requires authors to obtain permission from the copyright holder to reproduce any material that (1) they did not create themselves and/or (2) has been previously published, to include the authors' own work for which copyright was transferred to an entity other than ASCE. Each author has a responsibility to identify materials that require permission by including a citation in the figure or table caption or in extracted text. Materials re-used from an open access repository or in the public domain must still include a citation and URL, if applicable. At the time of submission, authors must provide verification that the copyright owner will permit re-use by a commercial publisher in print and electronic forms with worldwide distribution. For Conference Proceeding manuscripts submitted through the ASCE online submission system, authors are asked to verify that they have permission to re-use content where applicable. Written permissions are not required at submission but must be provided to ASCE if requested. Regardless of acceptance, no manuscript or part of a manuscript will be published by ASCE without proper verification of all necessary permissions to re-use. ASCE accepts no responsibility for verifying permissions provided by the author. Any breach of copyright will result in retraction of the published manuscript.

I, the corresponding author, confirm that all of the content, figures (drawings, charts, photographs, etc.), and tables in the submitted work are either original work created by the authors listed on the manuscript or work for which permission to re-use has been obtained from the creator. For any figures, tables, or text blocks exceeding 100 words from a journal article or 500 words from a book, written permission from the copyright holder has been obtained and supplied with the submission.

SARA AMOROSO	Sara Amoroso	11/09/2017
Print name	Signature	Date

III. Copyright Transfer

ASCE requires that authors or their agents assign copyright to ASCE for all original content published by ASCE. The author(s) warrant(s) that the above-cited manuscript is the original work of the author(s) and has never been published in its present form.

The undersigned, with the consent of all authors, hereby transfers, to the extent that there is copyright to be transferred, the exclusive copyright interest in the above-cited manuscript (subsequently called the "work") in this and all subsequent editions of the work (to include closures and errata), and in derivatives, translations, or ancillaries, in English and in foreign translations, in all formats and media of expression now known or later developed, including electronic, to the American Society of Civil Engineers subject to the following:

- The undersigned author and all coauthors retain the right to revise, adapt, prepare derivative works, present orally, or distribute the work, provided that all such use is for the personal noncommercial benefit of the author(s) and is consistent with any prior contractual agreement between the undersigned and/or coauthors and their employer(s).
- No proprietary right other than copyright is claimed by ASCE.
- If the manuscript is not accepted for publication by ASCE or is withdrawn by the author prior to publication (online or in print), or if the author opts for open-access publishing during production (journals only), this transfer will be null and void.
- Authors may post a PDF of the ASCE-published version of their work on their employers' ***Intranet*** with password protection. The following statement must appear with the work: "This material may be downloaded for personal use only. Any other use requires prior permission of the American Society of Civil Engineers."
- Authors may post the ***final draft*** of their work on open, unrestricted Internet sites or deposit it in an institutional repository when the draft contains a link to the published version at www.ascelibrary.org. "Final draft" means the version submitted to ASCE after peer review and prior to copyediting or other ASCE production activities; it does not include the copyedited version, the page proof, a PDF, or full-text HTML of the published version.

Exceptions to the Copyright Transfer policy exist in the following circumstances. Check the appropriate box below to indicate whether you are claiming an exception:

☐ **U.S. GOVERNMENT EMPLOYEES:** Work prepared by U.S. Government employees in their official capacities is not subject to copyright in the United States. Such authors must place their work in the public domain, meaning that it can be freely copied, republished, or redistributed. In order for the work to be placed in the public domain, ALL AUTHORS must be official U.S. Government employees. If at least one author is not a U.S. Government employee, copyright must be transferred to ASCE by that author.

☐ **CROWN GOVERNMENT COPYRIGHT:** Whereby a work is prepared by officers of the Crown Government in their official capacities, the Crown Government reserves its own copyright under national law. If ALL AUTHORS on the manuscript are Crown Government employees, copyright cannot be transferred to ASCE; however, ASCE is given the following nonexclusive rights: (1) to use, print, and/or publish in any language and any format, print and electronic, the above-mentioned work or any part thereof, provided that the name of the author and the Crown Government affiliation is clearly indicated; (2) to grant the same rights to others to print or publish the work; and (3) to collect royalty fees. ALL AUTHORS must be official Crown Government employees in order to claim this exemption in its entirety. If at least one author is not a Crown Government employee, copyright must be transferred to ASCE by that author.

☐ **WORK-FOR-HIRE:** Privately employed authors who have prepared works in their official capacity as employees must also transfer copyright to ASCE; however, their employer retains the rights to revise, adapt, prepare derivative works, publish, reprint, reproduce, and distribute the work provided that such use is for the promotion of its business enterprise and does not imply the endorsement of ASCE. In this instance, an authorized agent from the authors' employer must sign the form below.

☐ **U.S. GOVERNMENT CONTRACTORS:** Work prepared by authors under a contract for the U.S. Government (e.g., U.S. Government labs) may or may not be subject to copyright transfer. Authors must refer to their contractor agreement. For works that qualify as U.S. Government works by a contractor, ASCE acknowledges that the U.S. Government retains a nonexclusive, paid-up, irrevocable, worldwide license to publish or reproduce this work for U.S. Government purposes only. This policy DOES NOT apply to work created with U.S. Government grants.

I, the corresponding author, acting with consent of all authors listed on the manuscript, hereby transfer copyright or claim exemption to transfer copyright of the work as indicated above to the American Society of Civil Engineers.

SARA AMOROSO

Print Name of Author or Agent

Sara Amoroso 11/09/2017

Signature of Author of Agent Date

More information regarding the policies of ASCE can be found at http://www.asce.org/authorsandeditors